Milling and meandering: Flocking dynamics of stochastically interacting agents with a field of view

Trilochan Bagarti and Shakti N. Menon*
The Institute of Mathematical Sciences, CIT Campus, Taramani, Chennai 600113, India

(Received 10 May 2018; published 19 July 2019)

We introduce a stochastic agent-based model for the flocking dynamics of self-propelled particles that exhibit nonlinear velocity-alignment interactions with neighbors within their field of view. The stochasticity in the dynamics is spatially heterogeneous and arises implicitly from the nature of the interparticle interactions. We observe long-time spatial cohesion in the emergent flocking dynamics, despite the absence of attractive forces that explicitly depend on the relative positions of particles. The wide array of flocking patterns exhibited by this model are characterized by identifying spatially distinct clusters and computing their corresponding angular momenta.

DOI: 10.1103/PhysRevE.100.012609

I. INTRODUCTION

The collective movement of large groups of microorganisms, insects, birds, and mammals are amongst the most spectacular examples of self-organized phenomena in the natural world [1,2]. Species across a range of length scales exhibit a rich variety of collective patterns of motion that are united by similar underlying characteristics [3,4]. Advances in experimental techniques for investigating flocking [5] has sustained interest in uncovering the principles that underpin this emergent phenomenon. For instance, recent experiments have demonstrated that pairwise interactions motivated by biological goals play a crucial role in determining insect swarming patterns [6]. Flocks may fundamentally be viewed as dry active matter, namely systems of self-propelled particles that do not exhibit conservation of momentum [7], and their dynamics can be understood as a process similar to the long-range ordering of interacting particles [8]. Following the seminal work of Vicsek *et al.* [9,10], the dominant paradigm in models of flocking is that stochasticity in the dynamics can be accounted for through external noise (either additive or multiplicative). However, this approach is only appropriate when fluctuations arise from the surrounding media, for instance, in a system of Brownian particles. In contrast, experimental evidence suggests that the dominant contribution to the stochasticity in flocks arises from variability in the behavior of individual particles [11,12]. Furthermore, the collective dynamics of a swarm is known to be density-dependent [13,14], which tacitly suggests that variations in individual behavior may have a cumulative impact. Indeed, flocks may exhibit ordered macroscopic dynamics even if the behavior of individual particles is subject to noise [15]. Hence it is of significant interest to consider the emergent flocking behavior in a system where stochasticity arises purely from the uncertainties at the level of interparticle interactions.

In situations where individual particles are unable to uniformly survey their neighborhood due to physiological or other constraints, their interactions would be limited to neighbors that lie within a field of view [16]. It has been observed that even a minimal assumption of fore-aft asymmetry can significantly impact the collective dynamics of a flock [17]. Furthermore, a range of flocking patterns can be observed in a system with position-dependent short range interactions restricted by a vision cone [18]. Recently, we demonstrated that similar constraints on the field of view of a particle in a two-dimensional lattice model of flocking can yield a jamming transition even at extremely low particle densities [19]. Recent studies have investigated the dynamics of flocks that evolve via stochastic asynchronous update rules with explicit alignment and repulsion [20,21], and the effect of a field of view in Vicsek-like systems [22,23]. However, there remain open questions as to the nature of emergent dynamics when the stochasticity is not additive, but arises from uncertainties in the alignment of each particle with a neighbor in its field of view. Moreover, while certain types of position-dependent interactions can facilitate cohesion in a flock [24–26], it is intriguing to consider how this outcome might be achieved with velocity alignments alone. This would help shed light on the minimal conditions that underlie the emergence of cohesion in complex flocking behavior. Furthermore, while some flocking models have incorporated the acceleration of particles to describe short-term memory [27], collision avoidance [28], consensus decision making [29], and other experimentally observed features [30], the role of position-independent stochastic acceleration remains to be established.

In order to address these questions, we propose in this article a paradigm for flocking in which long-time spatial cohesion can emerge through a stochastic acceleration, despite the absence of attractive forces or explicit confinement. While a Langevin dynamics approach, where the deterministic and fluctuating components of motion are assumed to be separable, is used to study interacting particles in the presence of external noise, its validity in the context of flocking has not been established. In contrast, we explicitly consider a situation where, at each instant, particles interact with a single randomly chosen neighbor in their field of view through stochastic velocity alignments. Hence noise in this

*Corresponding author: shakti@imsc.res.in

system is spatially heterogeneous and is intrinsically linked to the dynamics of individual particles. We assume that the strength of interaction between a chosen pair of particles is independent of their relative positions and depends only on their instantaneous velocities, as opposed to the typical assumption of two-body or mean-field interactions. Finally, we present an algorithm that determines the spatially distinct clusters of the flock and their associated angular momenta.

II. MODEL

We consider an agent-based model of N interacting point-like particles moving in two dimensions. The state of each agent i at a time step t is described by its position $\mathbf{x}_i(t)$ and velocity $\mathbf{v}_i(t)$. The dynamics of the system is governed by the following update rule: at each time step t, an agent i interacts with a randomly chosen agent j with a specified probability $p(\mathbf{x}_j(t), \mathbf{v}_j(t)|\mathbf{x}_i(t), \mathbf{v}_i(t))$, defined later, leading to a change in its velocity. If it does not find any agent to interact with, it instead moves a distance $|\mathbf{v}_i(t)|$ in a random direction. The velocity $\mathbf{v}_i(t)$ and position $\mathbf{x}_i(t)$ are updated as

$$\mathbf{v}_i(t+1) = \mathbf{v}_i(t) + \mathbf{a}_i(t), \tag{1a}$$

$$\mathbf{x}_i(t+1) = \mathbf{x}_i(t) + \mathbf{v}_i(t+1). \tag{1b}$$

Here, $\mathbf{a}_i(t)$ is the agent's acceleration and is given by

$$\mathbf{a}_i(t) = \begin{cases} -\mathbf{v}_i(t) + |\mathbf{v}_i(t)|\,\hat{\boldsymbol{\eta}}, & \text{if } \Omega_i = \emptyset, \\ \alpha[\mathbf{v}_j(t) - \mathbf{v}_i(t) + f(\mathbf{v}_j(t) + \mathbf{v}_i(t))], & \text{otherwise,} \end{cases} \tag{2}$$

where Ω_i is the set of all agents with which agent i may interact, the coefficient $\alpha < 1$ is the strength of interaction, and $\hat{\boldsymbol{\eta}}$ is chosen from a uniform random distribution of vectors on the unit circle. Note that the velocity has the dimension of length. The initial condition is specified as $\mathbf{x}_i(0) = \mathbf{x}_i^0$ and $\mathbf{v}_i(0) = \mathbf{v}_i^0$ for all $i = 1, 2, \ldots, N$.

We note from Eq. (1a) that, when $\Omega_i \neq \emptyset$, the velocity update is dependent on the randomly chosen agent j. The linear term $\alpha(\mathbf{v}_j - \mathbf{v}_i)$ in Eq. (2) describes an alignment interaction, while the nonlinear term $f(\mathbf{v}_j + \mathbf{v}_i)$ keeps the velocity close to a critical value $\mathbf{v}_c$, i.e., it ensures that the flock maintains a constant average speed. Assuming $|\mathbf{v}_c| = 1$, we consider $f(\mathbf{v}) := \mathbf{v}(1 - |\mathbf{v}|)/(1 + |\mathbf{v}|^\beta)$ with $\beta = 3$. Note that, for large $|\mathbf{v}|$, $f(\mathbf{v}) \sim 1/|\mathbf{v}|^{\beta-2}$. So when $\mathbf{v}_j + \mathbf{v}_i$ is very small, or very large, the linear velocity-alignment term of the acceleration is dominant.

When the field of view of agent i is nonempty, i.e., $\Omega_i \neq \emptyset$, its velocity at time step $t+1$ is

$$\mathbf{v}_i(t+1) = \mathbf{v}_i(t) + \alpha[\mathbf{v}_j(t) - \mathbf{v}_i(t) + f(\mathbf{v}_j(t) + \mathbf{v}_i(t))].$$

For the functional form that we consider, we see that $f(\mathbf{v}_j + \mathbf{v}_i)$ vanishes at $|\mathbf{v}_j + \mathbf{v}_i| = 0$, 1, and ∞, which implies that the velocity $\mathbf{v}_i(t+1) \simeq \mathbf{v}_i(t) + \alpha[\mathbf{v}_j(t) - \mathbf{v}_i(t)]$ near these values. The case $|\mathbf{v}_j + \mathbf{v}_i| = 0$ corresponds to a situation where the velocities of particles i and j have identical magnitudes and opposite directions. In this scenario, the resulting velocity update effectively prevents a direct collision. To understand the case $|\mathbf{v}_j + \mathbf{v}_i| = 1$, let us assume that $|\mathbf{v}_i + \mathbf{v}_j| = 1 + \epsilon$, where $|\epsilon| \ll 1$. In this situation, we see that

$$f(\mathbf{v}_i + \mathbf{v}_j) = \frac{(\mathbf{v}_i + \mathbf{v}_j)[1 - (1+\epsilon)]}{1 + (1+\epsilon)^3} \simeq \frac{-\epsilon(\mathbf{v}_i + \mathbf{v}_j)}{2}.$$

Substituting this expression into Eq. (2), we find that the acceleration is

$$\mathbf{a}_i \simeq \alpha\Big(1 - \frac{\epsilon}{2}\Big)\mathbf{v}_j - \alpha\Big(1 + \frac{\epsilon}{2}\Big)\mathbf{v}_i.$$

Using the velocity update expression from Eq. (1), we see that $|\mathbf{v}_i|_{\epsilon\neq 0} < |\mathbf{v}_i|_{\epsilon=0}$ if $\epsilon > 0$ and $|\mathbf{v}_i|_{\epsilon\neq 0} > |\mathbf{v}_i|_{\epsilon=0}$ if $\epsilon < 0$. This implies that, for $\epsilon > 0$, the agent slows down, whereas, for $\epsilon < 0$, it moves faster. In other words, the nonlinear term $f(\mathbf{v}_j + \mathbf{v}_i)$ ensures that the agent's speed remains close to that of the specified mean value.

For our current investigation, we assume that every agent i has a field of view, symmetric around its direction of motion, that is delimited by a maximum bearing angle $\theta_{\max}$. Such an assumption is valid for a wide class of systems where agents are intrinsically polar, such as in bird flocks or in animal herds. The probability $p(\mathbf{x}_j, \mathbf{v}_j|\mathbf{x}_i, \mathbf{v}_i)$ that an agent i interacts with an agent $j \in \Omega_i$ may be specified in terms of weights $\omega_{i,j}$. In the absence of any external signals, or any intrinsic directional bias, it is reasonable to assume that an agent in a flock would align its direction of motion with an agent in its direct line of sight with a higher probability compared to an agent lying near the edge of its field of view. We assume that a given agent mostly interacts with agents separated from it by an optimal interaction length, and that the probability that it randomly selects an agent lying very close to or very far away from itself is negligible. With these properties in mind we assume the following weight function:

$$\omega_{i,j} = |\mathbf{x}_i - \mathbf{x}_j|\, e^{-\frac{|\mathbf{x}_i - \mathbf{x}_j|^2}{2\sigma^2}} \big(1 - \theta_{i,j}^2/\theta_{\max}^2\big), \tag{3}$$

if $\theta_{i,j} \leqslant \theta_{\max}$ and $\omega_{i,j} = 0$ for $\theta_{i,j} > \theta_{\max}$, where σ is the mean interaction length and $\theta_{i,j}$ is the angle between the velocity $\mathbf{v}_i$ and the vector $\mathbf{x}_j - \mathbf{x}_i$. Given this weight function, the probability can be written as $p(\mathbf{x}_j, \mathbf{v}_j|\mathbf{x}_i, \mathbf{v}_i) = \omega_{i,j}/\sum_{k\in\Omega_i}\omega_{i,k}$. The nature of this field of view is illustrated in Fig. 1. An agent j within this field of view is picked by i with a probability that is related to the distance between them, as well as the angle between the velocity of i and the line connecting the two agents. If the field of view of agent i is empty, it performs a random rotation.

In the limiting case $\theta_{\max} = \pi$, there are no random rotations as, by definition, we would have $\Omega_i \neq \emptyset\ \forall\ i$. In this situation any initial randomness will eventually get redistributed over the whole population and it is expected that the velocities will converge to that of the initial mean velocity. Furthermore, here an agent i has the highest likelihood to align with any neighbor j that approximately lies at a distance $|\mathbf{x}_i - \mathbf{x}_j| = \sigma$ (i.e., where $\omega_{i,j}$ is at its maximum). Hence, in our simulations, we assume that the initial positions $\mathbf{x}_i^0$ are such that the agents are uniformly distributed over a circular region of radius σ and the velocities $\mathbf{v}_i^0$ are chosen from a uniform distribution over the range [0,1]. In addition, we note that Ω_i is not invariant under the transformation $\mathbf{v}_i \to -\mathbf{v}_i$, as a consequence of the inherent anisotropy of the field of view, which hence breaks the time-reversal symmetry. However, such a transformation

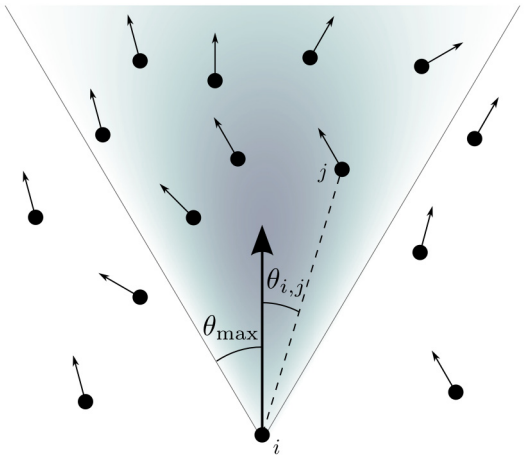

FIG. 1. Schematic of the field of view of an agent in our model. The intensity of color in a given region is related to the the probability with which a given agent i chooses an agent j that lies in that region. Each agent has the highest probability of interacting with agents that lie at a distance σ along its direction of motion. Similarly, the intensity reduces as the angle $\theta_{i,j}$ between the velocity of i and the line connecting the agents approaches the maximum bearing angle $\theta_{\max}$. Thus an agent i is most likely to align with an agent that is near its direct line of sight and which is separated by a distance of around σ.

will not affect the nature of the pattern at the scale of the entire flock.

III. RESULTS

Upon varying the interaction strength α, mean interaction length σ, and the maximum bearing angle $\theta_{\max}$ over a range of values for a system of $N = 10^3$ agents, we find that the model exhibits a wide range of patterns (see Fig. 2). From our numerical simulations, we find that the resulting patterns can sustain their cohesiveness over a very long period of time ($t \gtrsim 10^6$ steps). These observed patterns include an extended bandlike flock that can move ballistically for long durations [Fig. 2(a)], a very large and narrow closed trail pattern [Fig. 2(b)], a spatially extended wriggling pattern [Fig. 2(c)], a flock that exhibits a milling, or vortexlike, pattern [Fig. 2(d)], and a flock with a meandering center of mass, and rotating profile, that remains confined to a small region of space [Fig. 2(e)]. Similar milling patterns have been observed in diverse contexts across the natural world [31–34], including fish schools and ant mills. We have verified that qualitatively similar flocking patterns can be obtained even for much larger system sizes [see Supplemental Material [35] which also includes movies of the patterns displayed in Figs. 2(b_1)–2(e_1)]. Furthermore, in addition to the patterns displayed in Fig. 2, this system can exhibit multiple interacting clusters. To illustrate this we have plotted in Figs. 2(a_3)–2(e_3) the temporal variation of the angular momentum per particle, $\mathbf{L} = N^{-1}\sum_i(\mathbf{x}_i - \bar{\mathbf{x}}) \times \mathbf{v}_i$ for the corresponding flocking patterns, where $\bar{\mathbf{x}}(t) = N^{-1}\sum_i \mathbf{x}_i(t)$ is the center of mass of the flock. We observe that this quantity exhibits remarkably distinct temporal profiles for each of the displayed patterns and captures the spontaneous switching and reversal in the direction of rotation of the flock, which manifests as a change in the sign of $\mathbf{L}$.

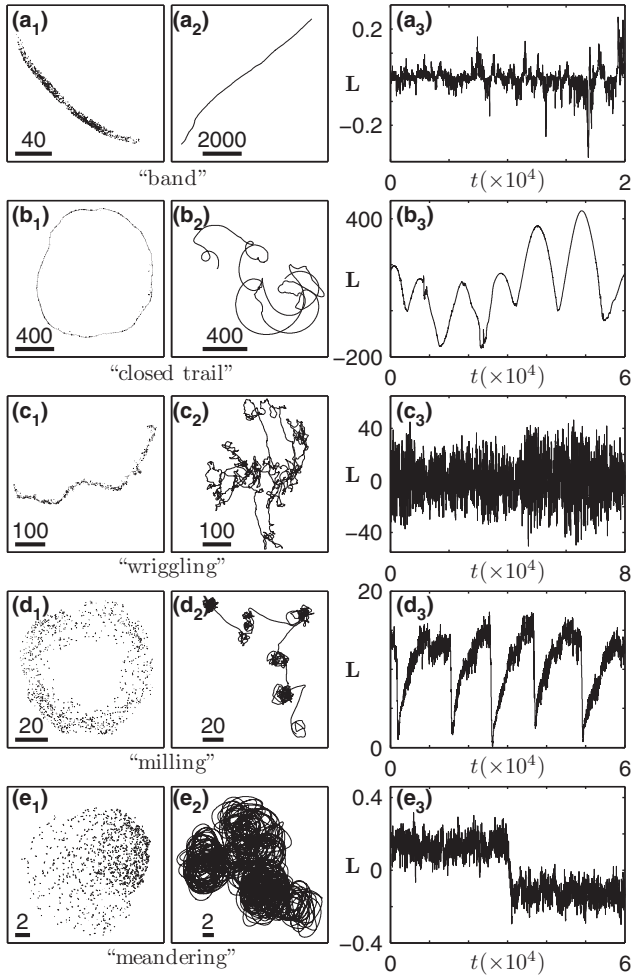

FIG. 2. Examples of the spatially contiguous dynamical flocking patterns exhibited by the model for a system of $N = 10^3$ agents. In each row the left panel displays a snapshot of the flock, the right panel displays the angular momentum per particle $\mathbf{L}$ over a duration of time, and the middle panel displays the corresponding trajectory of the center of mass of the flock $\bar{\mathbf{x}}(t)$ over the same duration. (a_1)–(a_3) Agents moving in a band for the case $\sigma = 6$, $\theta_{\max} = 90°$, and $\alpha = 0.1$. (b_1)–(b_3) Agents moving in a closed trail for the case $\sigma = 3$, $\theta_{\max} = 50°$, and $\alpha = 0.1$. (c_1)–(c_3) Agents moving in a wriggling pattern for the case $\sigma = 5$, $\theta_{\max} = 40°$, and $\alpha = 0.8$. (d_1)–(d_3) Agents moving in a milling pattern for the case $\sigma = 1$, $\theta_{\max} = 20°$, and $\alpha = 0.025$. (e_1)–(e_3) Agents moving in a flock with a meandering center of mass for the case $\sigma = 3$, $\theta_{\max} = 15°$, and $\alpha = 0.02$. The numbered solid bars in the left and middle panels of every row provide a measure of spatial distance in each case.

In Figs. 2(a_2)–2(e_2), the trajectories of the center of mass of the flock, $\bar{\mathbf{x}}(t)$, illustrate the diversity of collective dynamics that this model is capable of exhibiting. These range from near-ballistic motion in the case of the bandlike patterns [Fig. 2(a_2)] to winding behavior with occasional long excursions, similar to that of a correlated random walk, in the case of the milling pattern [Fig. 2(e_2)]. To discern the macroscopic features of these trajectories, we discard an initial transient period of duration $t_0 = 10^3$ and compute the probability distribution function $\mathcal{P}(s,t)$, where $s = |\bar{\mathbf{x}}(t) - \bar{\mathbf{x}}(t_0)|$, and the mean square displacement (MSD) of the center of mass, $\langle s^2 \rangle$.

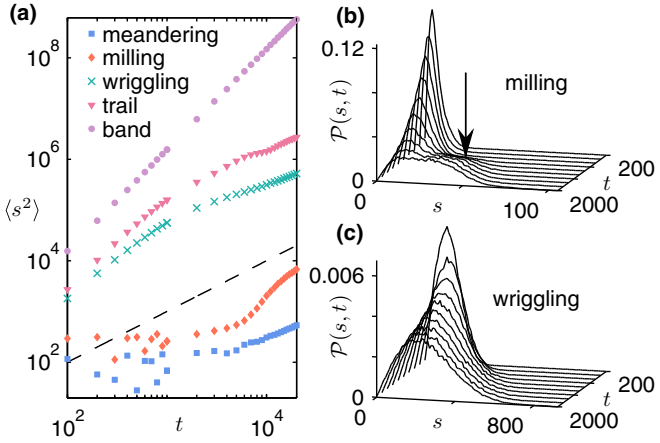

FIG. 3. Statistics of the center of mass trajectories. (a) Time-dependence of the average mean-squared displacement (MSD) of the center of mass $\langle s^2 \rangle$, calculated over 10^4 trials, for each of the five sets of parameter values considered in Fig. 2. The dashed line, shown for reference, indicates the MSD for the case of normal diffusion. (b), (c) The probability distribution function $\mathcal{P}(s,t)$, calculated over 5×10^4 trials, shown over a range of displacements s and time t for the cases (b) $\sigma = 1$, $\theta_{\max} = 20^\circ$, $\alpha = 0.025$ (a milling pattern) and (c) $\sigma = 5$, $\theta_{\max} = 40^\circ$, $\alpha = 0.8$ (a wriggling pattern). The arrow in panel (b) indicates a large excursion.

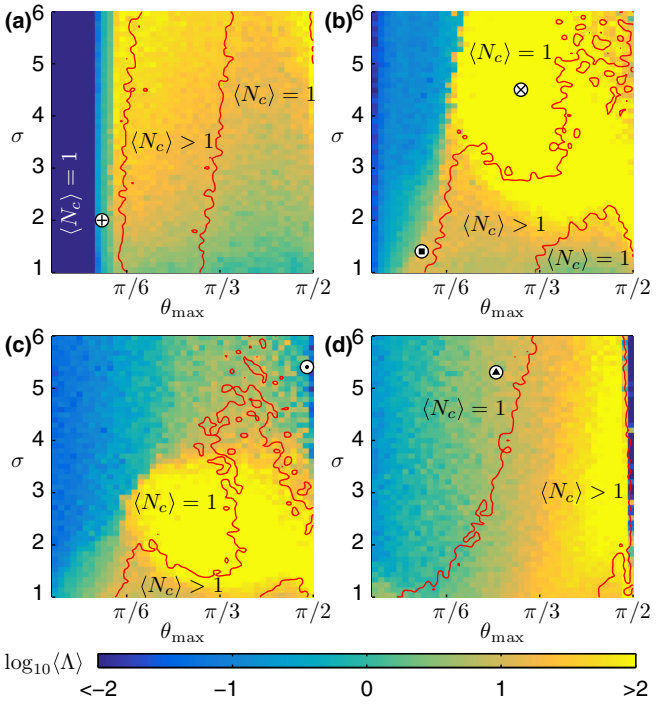

FIG. 4. Parameter space diagrams obtained using the cluster-finding algorithm described in the text. The ensemble-averaged quantities $\langle N_c \rangle$ and $\langle \mathbf{\Lambda} \rangle$ are computed over a range of values of the mean interaction length σ, interaction strength α, and the maximum bearing angle $\theta_{\max}$, and are averaged over 10 trials. The four panels correspond to (a) $\alpha = 0.01$, (b) $\alpha = 0.05$, (c) $\alpha = 0.1$, and (d) $\alpha = 0.5$. In each, we display (in log scale) the dependence of the average angular momentum of the flock $\langle \mathbf{\Lambda} \rangle$ on system parameters, along with contour lines that demarcate the regimes where the flock is characterized by a single cluster ($\langle N_c \rangle = 1$) and multiple clusters ($\langle N_c \rangle > 1$). The black markers within white circles in each panel indicate locations in the parameter space where we observe a meandering pattern [(a) plus sign], a milling pattern [(b) filled square], a closed trail [(b) cross], a band pattern [(c) filled circle], and a wriggling pattern [(d) filled triangle]. A more detailed exploration of the parameter space, with snapshots of the patterns obtained, is provided in the Supplemental Material [35].

While the trail and wriggling patterns show a superdiffusive behavior at small time scales, they appear to converge to normal diffusion $\langle s^2 \rangle \sim t$ asymptotically [cf. dashed line in Fig. 3(a)]. In contrast, the milling and the meandering patterns are initially subdiffusive and asymptotically converge to normal diffusion, while the band pattern is superdiffusive at all times. The probability density function $\mathcal{P}(s,t)$ for the milling and the wriggling patterns are shown in Figs. 3(b) and 3(c). We find that the patterns show a qualitatively similar decay of $\mathcal{P}(s,t)$ at small times. However, as indicated by an arrow in Fig. 3(b), the center of mass of the milling pattern exhibits a higher probability of large excursions at later times, which corresponds to intervals where rotation ceases due to an internal reorganization of the flock.

While a nonzero mean velocity of the flock corresponds to ordered motion, indicating a band pattern, a zero mean velocity may either correspond to randomly moving agents or to an ordered swirling flock. Furthermore, for certain choices of the system parameters, the flock comprises several clusters. Hence simple scalar order parameters such as the mean velocity of the flock would only permit us to distinguish ordered and disordered dynamics. In order to characterize the wide array of flocking patterns observed in our simulations, we would need information regarding translational and rotational motion of the individual clusters of the flock.

To this end, we characterize the dynamics in terms of the distinct (contiguous) clusters of particles through the following cluster-finding algorithm and compute their associated angular momenta. We define the resolution length $R = \lambda R_{\max}$, where $0 < \lambda \leqslant 1$ and $R_{\max}$ is the maximum separation between any two particles in the flock at time t. At the length scale $R_{\max}$ the system can be viewed as comprising a single cluster that encompasses the entire flock. For the chosen length scale R, we first compute $r_{i,j} = |\mathbf{x}_i(t) - \mathbf{x}_j(t)|$ for all $i, j \neq i$ and group the agents into distinct clusters such that a pair of agents (i, j) in any given cluster satisfies the condition $r_{i,j} \leqslant R$. Next, we regroup the agents such that if $r_{i,j} \leqslant R$ and $r_{j,k} \leqslant R$ but $r_{i,k} > R$, then the agents i, j, and k are assumed to belong to the same cluster. The resolution length R hence provides a lower bound on the spatial separation of any pair of detected clusters. Once the individual clusters c_i (of size N_i) have been determined, we define N_c to be the minimum number of clusters whose collective population exceeds 90% of N, i.e., $N_c = \min\{n : 0.9N \leqslant \sum_{i=1}^{n} N_i, 1 \leqslant n \leqslant N\}$. The center of mass of a cluster c_i is defined as $\bar{\mathbf{x}}_i = N_i^{-1} \sum_{j \in c_i} \mathbf{x}_j$ and the corresponding angular momentum about the center of mass is $\mathbf{L}_i = N_i^{-1} \sum_{j \in c_i} (\mathbf{x}_j - \bar{\mathbf{x}}_i) \times \mathbf{v}_j$. We then compute the quantity $\Lambda = N_c^{-1} \sum_{i=1}^{N_c} |\mathbf{L}_i|$, where the absolute value sign takes into account the fact that the flock may contain clusters that swirl in opposite directions. A pseudocode of this algorithm is provided in the Supplemental Material [35]. In

our study we have used $\lambda = 2^{-4}$, and find that the outcome is robust with respect to a small variation $R \pm \delta$, where $\delta \in (0, R/2)$. Note that as $\lambda \to 0$ we would, by definition, find N clusters that each comprise a single agent.

In Fig. 4 we display a parameter space diagram that quantifies the flocking dynamics in terms of two ensemble averaged quantities, namely angular momentum $\langle \Lambda \rangle$ and the number of clusters $\langle N_c \rangle$, over a range of values of σ, $\theta_{\max}$, and α. The contour lines demarcate regimes where the flocking pattern is characterized by a single ($\langle N_c \rangle = 1$) and multiple clusters ($\langle N_c \rangle > 1$). A general observation from Fig. 4 is that, at low values of $\theta_{\max}$, the mean angular momentum is very low, regardless of σ or α and that the corresponding patterns are characterized by a single diffusive cluster. Such cohesive but highly disordered flocking behavior has been reported earlier in the context of midge swarming patterns [36]. Patterns with very high angular momentum, which typically correspond to single or multiple closed trails, are observed for larger values of α. For $\alpha = 0.01$ we observe multiple clusters over an intermediate range of values of $\theta_{\max}$. Multiple clusters are also observed for larger values of α, although the regimes where they occur exhibit a more complex dependence on $\theta_{\max}$. Snapshots of the collective patterns obtained over the entire range of parameter values considered in Fig. 4 are presented in the Supplemental Material [35].

IV. CONCLUSION

A crucial feature of our model is that particles at the edge of the flock are subject to more randomness, as there is a relatively higher probability that their field of view is empty. In contrast, the interior of the flock is comparatively ordered through a process of self-organization, due to the increased likelihood of alignment interactions. In addition to facilitating cohesion, this may help explain the apparent symmetry of several of the patterns (cf. milling, meandering, and closed trails), as flocks with smoother boundaries have much lower stochasticity overall. In this regard, the existence of the wriggling pattern, which has a rougher boundary, is due to the fact that the stochasticity at the edge is reduced for larger values of σ. These results are intriguing in light of recent observations that the boundary of a flock plays an important role in its emergent dynamics [37]. Additionally, we note that, as the alignment probability in our model is dependent on $\theta_{\max}$, there is an inherent spatial anisotropy in the stochastic interactions. Specifically, for $\theta_{\max} < \pi/2$ agents do not interact with neighbors that lie directly behind them. This may relate to the emergence of milling patterns in our model, as previous flocking models that reported such patterns have typically incorporated such a "blind zone" for agents [31,38–40].

In conclusion, our model provides a mechanism through which stochasticity arises intrinsically from the interactions between agents and yields a rich array of flocking patterns that exhibit long-time cohesion. This framework can, in principle, be generalized to the case of stochastic many-body interactions. In addition, our algorithm for identifying and computing the angular momenta of spatially distinct clusters of a flock may help provide additional insights into other flocking systems, both theoretical and experimental. Furthermore, the model proposed here could be extended to describe pursuit and evasion in predator-prey systems [41], as well as incorporate the role of social hierarchy in flocks [42–44] and the role of memory on the emergent flocking behavior.

ACKNOWLEDGMENTS

We would like to thank Abhijit Chakraborty, Niraj Kumar, V. Sasidevan, and Gautam Menon for helpful discussions. S.N.M. is supported by the IMSc Complex Systems Project (12th Plan). The simulations and computations required for this work were supported by the Institute of Mathematical Science's High Performance Computing facility (hpc.imsc.res.in) [nandadevi], which is partially funded by the Department of Science and Technology, Government of India.

[1] T. Vicsek and A. Zafeiris, Phys. Rep. **517**, 71 (2012).
[2] D. J. Sumpter, Philos. Trans. R. Soc. B **361**, 5 (2006).
[3] *Animal Groups in Three Dimensions*, edited by J. K. Parrish and W. M. Hamner (Cambridge University Press, Cambridge, UK, 1997).
[4] G. I. Menon, in *Rheology of Complex Fluids*, edited by J. Krishnan, A. Deshpande, and P. Kumar (Springer, New York, 2010).
[5] A. Cavagna, I. Giardina, and T. S. Grigera, Phys. Rep. **728**, 1 (2018).
[6] J. G. Puckett, R. Ni, and N. T. Ouellette, Phys. Rev. Lett. **114**, 258103 (2015).
[7] M. C. Marchetti, J. F. Joanny, S. Ramaswamy, T. B. Liverpool, J. Prost, M. Rao, and R. A. Simha, Rev. Mod. Phys. **85**, 1143 (2013).
[8] A. Cavagna and I. Giardina, Annu. Rev. Condens. Matter Phys. **5**, 183 (2014).
[9] T. Vicsek, A. Czirók, E. Ben-Jacob, I. Cohen, and O. Shochet, Phys. Rev. Lett. **75**, 1226 (1995).
[10] F. Ginelli, Eur. Phys. J.: Spec. Top. **225**, 2099 (2016).
[11] L. M. Aplin, D. R. Farine, R. P. Mann, and B. C. Sheldon, Proc. R. Soc. B **281**, 20141016 (2014).
[12] M. del Mar Delgado, M. Miranda, S. J. Alvarez, E. Gurarie, W. F. Fagan, V. Penteriani, A. di Virgilio, and J. M. Morales, Philos. Trans. R. Soc. B **373**, 20170008 (2018).
[13] J. Buhl, D. J. T. Sumpter, I. D. Couzin, J. J. Hale, E. Despland, E. R. Miller, and S. J. Simpson, Science **312**, 1402 (2006).
[14] C. A. Yates, R. Erban, C. Escudero, I. D. Couzin, J. Buhl, I. G. Kevrekidis, P. K. Maini, and D. J. T. Sumpter, Proc. Natl. Acad. Sci. USA **106**, 5464 (2009).
[15] T. Niizato and H. Murakami, PloS One **13**, e0195988 (2018).
[16] C. K. Hemelrijk and H. Hildenbrandt, Interface Focus **2**, 726 (2012).
[17] Q.-S. Chen, A. Patelli, H. Chaté, Y.-Q. Ma, and X.-Q. Shi, Phys. Rev. E **96**, 020601(R) (2017).
[18] L. Barberis and F. Peruani, Phys. Rev. Lett. **117**, 248001 (2016).
[19] S. N. Menon, T. Bagarti, and A. Chakraborty, Europhys. Lett. **117**, 50007 (2017).

[20] N. W. F. Bode, J. J. Faria, D. W. Franks, J. Krause, and A. J. Wood, Proc. R. Soc. B **277**, 3065 (2010).
[21] N. W. F. Bode, D. W. Franks, and A. J. Wood, J. R. Soc. Interface **8**, 301 (2011).
[22] B. M. Tian, H. X. Yang, W. Li, W. X. Wang, B. H. Wang, and T. Zhou, Phys. Rev. E **79**, 052102 (2009).
[23] Y.-J. Li, S. Wang, Z.-L. Han, B.-M. Tian, Z.-D. Xi, and B.-H. Wang, Europhys. Lett. **93**, 68003 (2011).
[24] G. Grégoire, H. Chaté, and Y. Tu, Physica D **181**, 157 (2003).
[25] G. Grégoire and H. Chaté, Phys. Rev. Lett. **92**, 025702 (2004).
[26] H. Chaté, F. Ginelli, G. Grégoire, and F. Raynaud, Phys. Rev. E **77**, 046113 (2008).
[27] P. Szabó, M. Nagy, and T. Vicsek, Phys. Rev. E **79**, 021908 (2009).
[28] L. Peng, Y. Zhao, B. Tian, J. Zhang, B. H. Wang, H. T. Zhang, and T. Zhou, Phys. Rev. E **79**, 026113 (2009).
[29] K. Bhattacharya and T. Vicsek, New J. Phys. **12**, 093019 (2010).
[30] S. Mishra, K. Tunstrøm, I. D. Couzin, and C. Huepe, Phys. Rev. E **86**, 011901 (2012).
[31] R. Lukeman, Y.-X. Li, and L. Edelstein-Keshet, Bull. Math. Biol. **71**, 352 (2008).
[32] U. Lopez, J. Gautrais, I. D. Couzin, and G. Theraulaz, Interface Focus **2**, 693 (2012).
[33] K. Tunstrøm, Y. Katz, C. C. Ioannou, C. Huepe, M. J. Lutz, and I. D. Couzin, PLoS Comput. Biol. **9**, e1002915 (2013).
[34] A. B. Sendova-Franks, N. R. Franks, and A. Worley, R. Soc. Open Sci. **5**, 180665 (2018).
[35] See Supplemental Material at http://link.aps.org/supplemental/10.1103/PhysRevE.100.012609 for pseudocode of the cluster-finding algorithm, figures illustrating that the results are robust at larger system sizes, snapshots of flocks obtained over a range of parameter values, and movies displaying the evolution of different flocking patterns.
[36] A. Okubo, Adv. Biophys. **22**, 1 (1986).
[37] A. Cavagna, I. Giardina, and F. Ginelli, Phys. Rev. Lett. **110**, 168107 (2013).
[38] I. D. Couzin, J. Krause, R. James, G. D. Ruxton, and N. R. Franks, J. Theor. Biol. **218**, 1 (2002).
[39] D. J. G. Pearce, A. M. Miller, G. Rowlands, and M. S. Turner, Proc. Natl. Acad. Sci. USA **111**, 10422 (2014).
[40] A. Costanzo and C. K. Hemelrijk, J. Phys. D **51**, 134004 (2018).
[41] P. Romanczuk, I. D. Couzin, and L. Schimansky-Geier, Phys. Rev. Lett. **102**, 010602 (2009).
[42] M. Nagy, Z. Ákos, D. Biro, and T. Vicsek, Nature (London) **464**, 890 (2010).
[43] B. Pettit, Z. Ákos, T. Vicsek, and D. Biro, Curr. Biol. **25**, 3132 (2015).
[44] M. C. Miguel, J. T. Parley, and R. Pastor-Satorras, Phys. Rev. Lett. **120**, 068303 (2018).